IEEE Photonics Journal
An IEEE Photonics Society Publication

Open Access

Design and Analysis of Ultra-Wideband Highly-Birefringent Bragg Layered Photonic Bandgap Fiber With Concave-Index Cladding

Volume 13, Number 3, June 2021

Hongyu Tan
Chaotan Sima
Botao Deng
Xiaohang Zhang
Guoqun Chen
Qianqing Yu
Jianghe Xu
Zhenggang Lian
Deming Liu

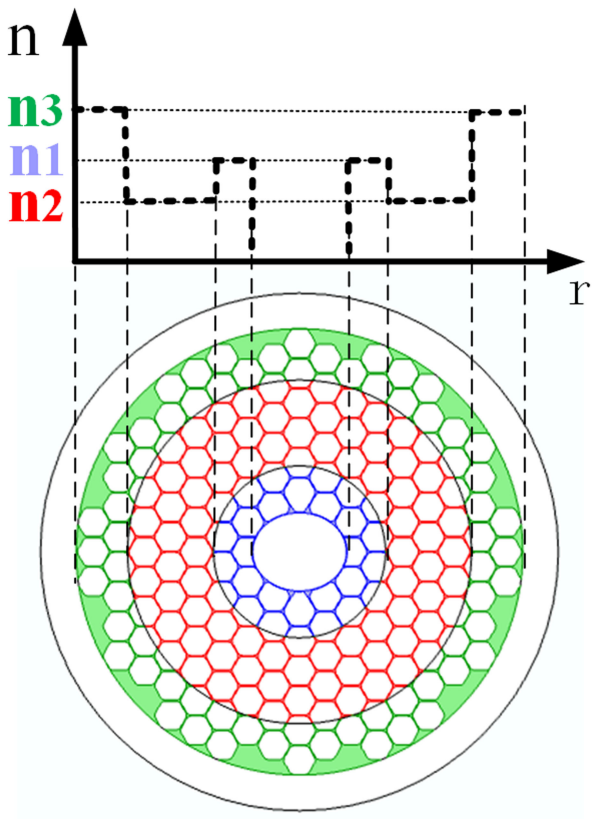

DOI: 10.1109/JPHOT.2021.3075446

Design and Analysis of Ultra-Wideband Highly-Birefringent Bragg Layered Photonic Bandgap Fiber With Concave-Index Cladding

Hongyu Tan,[1] Chaotan Sima ,[1] Botao Deng,[1] Xiaohang Zhang,[1] Guoqun Chen,[2] Qianqing Yu,[2] Jianghe Xu,[2] Zhenggang Lian ,[2] and Deming Liu[1]

[1]Next Generation Internet Access National Engineering Laboratory, School of Optical and Electronic Information, Huazhong University of Science and Technology, Wuhan 430074, China
[2]Yangtze Optical Electronics Company, Ltd. (YOEC), Wuhan 430205, China

DOI:10.1109/JPHOT.2021.3075446

Manuscript received February 14, 2021; revised April 17, 2021; accepted April 21, 2021. Date of publication April 26, 2021; date of current version May 10, 2021. This work was supported in part by the National Key R&D Program of China under Grant 2018YFF01011800, and in part by the National Natural Science Foundation of China under Grant 62075074. Corresponding author: Chaotan Sima (e-mail: smct@hust.edu.cn).

Abstract: A ultra-wideband highly-birefringent Bragg layered photonic bandgap fiber (BL-PBGF) with concave-index cladding is proposed and demonstrated, by incorporating PBG effect with Bragg multilayers for the first time to the best of our knowledge. The proposed BL-PBGF contains honeycomb capillary cladding and elliptical core with horizontal asymmetry for birefringence. By innovatively introducing three modified silica capillary layers with different refractive indices, the cladding with concave-convex refractive index distribution is combined, providing superior characteristics for optical polarization implementation, such as confinement loss, bending loss and birefringence. Results show that the confinement loss stays around 2 dB/km level within ultrawide 180 nm wavelength range, basically 3 times wider than conventional PBGF. The birefringence maintains at the order of 10^{-3} across the entire bandwidth and the maximum value reaches 2.5×10^{-3}. The bending loss at 1550 nm is significantly reduced to below one third of the conventional uniform index PBGF when the bending radius is less than 3.5 mm, and maintains below 1 dB/km level when the bending radius is beyond 10 mm. The proposed universal BL-PBGF has great potential in minimized freestanding fiber coil and small footprint fiber optical gyroscope applications.

Index Terms: Theory and design, photonic bandgap structures, photonic crystals, modeling.

1. Introduction

The highly-birefringent optical fiber, also named as polarization-maintaining fiber (PMF), has been widely used in optical sensing and optical communication since 1979 [1]. With the rapid development of communication systems and advanced sensing applications, novel PMFs are in need to meet demands of high birefringence as well as thermal and radiation stability in practical utilizations [2], [3]. The birth of photonic crystal fiber (PCF) paves the way for these requirements due to the flexibility and variety, such as geometry and distribution of air holes in the cross section

[4], [5]. Structural symmetry of the PCF could be interrupted by changing geometry and layout of core and cladding air holes, thereby obtaining high birefringence [6]–[11]. Birefringence could reach the level of 10^{-3} for commercial PMFs [12].

Furthermore, the hollow core photonic bandgap fiber (HC-PBGF) brings along benefits of light weight, long lifetime and irradiation resistance, which finds significant potentials for fiber optic gyroscopes (FOGs) [13]–[15]. In 2004, Chen *et al.* reported an anisotropy hollow-core photonic bandgap fiber [6], with group modal birefringence of 2.5×10^{-2} at 1550 nm and transmission loss of about 1500 dB/km from 1500 nm to 1625 nm. In 2014, Fini et al. reported a single-mode polarization-maintaining HC-PBGF [7], with about 10 dB/km loss from 1526 to 1540 nm and the minimum birefringent beat length of 7 mm, equivalent to the birefringence of 2.2×10^{-4}, while the transmission at 1550 nm was not designed and realized. In 2014, Michieletto *et al.* demonstrated a HC-PBGF with the cladding incorporating a row of partially collapsed holes to strip away unwanted surface modes [8], showing transmission loss of about 60 dB/km and group modal birefringence of 10^{-3} at 1550 nm. Considering polarization features, Serrão *et al.* designed a single-polarization hollow-core photonic bandgap fiber with reduced dimensions of a radial line of air-holes in 2013 [9], showing a high polarization dispersion loss (PDL $>$ 20 dB/m) with bandwidth of about 38 nm and the confinement loss of 0.1 dB/km at 1550 nm. In 2016, Chen et al. theoretically proposed a polarization-maintaining HC-PBGF with a quasi-elliptical core [10], with birefringence of 4.6×10^{-4} and confinement loss of 20 dB/km from 1460 nm to 1590 nm. In 2020, Cai et al. designed a thin-diameter polarization-maintaining HC-PBGF, with the loss of about 15 dB/km at 1550 nm and birefringence of 1.2×10^{-4} [11]. Nevertheless, bending characteristics of these PBGFs in literatures are to be considered and discussed. Regarding most recognized PMF applications in freestanding fiber coil and miniature fiber-optic gyroscopes [16], [17], optical characteristics including bending loss with small radius as well as wideband operation are also of straightforward interest and could be further investigated. To be noted, above-mentioned HC-PBGFs focused on geometrical composition and modification in micro-structures, merely with single uniform silica glass material ($n\approx1.45$).

Meanwhile, considering Bragg fibers and OmniGuide fibers [18], [19], the fiber core is normally surrounded by a multilayer cladding that consists of alternating layers having high contrast indices of refraction, allowing the light propagation in UV and far-infrared regions. The high and low indices in these periodic coaxial claddings are generally realized by different materials, such SiN and metal, instead of silica, which would bring along fiber fabrication challenges and loss issues.

In this paper, a ultra-wideband highly-birefringent Bragg layered photonic bandgap fiber (BL-PBGF) in use of concave-index cladding is proposed and demonstrated, by incorporating photonic bandgap effect with Bragg effect. Weak refractive index contrast (about 0.7%) in the concave index distribution is introduced to the PBG cladding structure. To the best of our knowledge this is the first time to introduce this Bragg type multilayer concept to the PBG holey fiber, which brings along notable optical benefits. The proposed BL-PBGF is simulated and analyzed by using the Finite Element Method (FEM) [20]–[23]. The confinement loss achieves as low as 1 dB/km for single mode operation around 1550 nm and remains below 2 dB/km in the ultrawide 180 nm wavelength range from 1450 nm to 1630 nm, basically 3 times wider than the conventional uniform index PBGF. More importantly, the bending loss of the proposed BL-PBGF becomes less than one third of the conventional PBGF when bending radius is below 3.5 mm and maintains below 1 dB/km when the bending radius is beyond 10 mm. The birefringence of this fiber can also be maintained at the order of 10^{-3} across the wide bandwidth and shows excellent polarization maintenance with small bending radius. These benefits provide great potential in the miniature freestanding fiber coil and small footprint FOG applications.

2. Principle and Structure

The cross-section of the proposed BL-PBGF is schematically shown in Fig. 1. The cladding employs the typical honeycomb air hole structure for the PBG effect. The elliptical hollow core structure is introduced by adjusting the ellipticity of the hollow core to enhance birefringence.

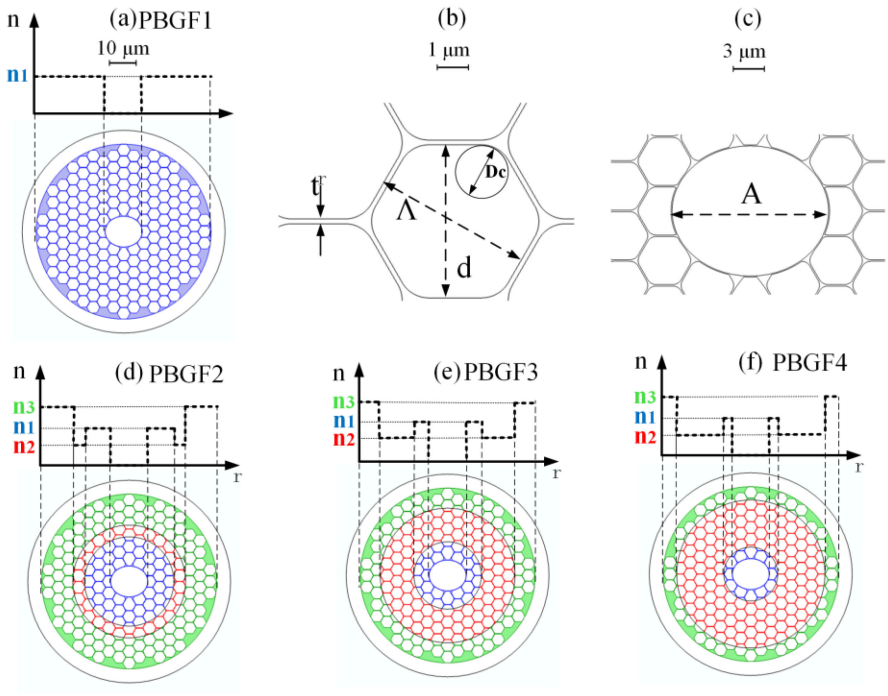

Fig. 1. The cross-section and multiplayer distributions of the proposed BL-PBGFs: (a) PBGF1 with uniform n_1, identical to conventional PBGF; (b) detailed cladding parameters of the fiber cross-section; (c) elliptical hollow core structure; (d) PBGF2; (e) PBGF3; (f) PBGF4.

It is acknowledged that the bandgap range and bandwidth are mainly determined by air-filling fraction *f*. Specially, the bandgap will shift toward shorter wavelengths when the air-filling fraction f increases and the relative bandwidth enlarges exponentially with f^2[24]. Here these parameters of the proposed PBGFs are designed to make the photonic bandgaps centered around 1550nm. The overall diameter of the photonic bandgap section is 73 μm, where the honeycomb cladding diameter is 63 μm, and the cladding air holes adopt a hexagonal or circular structure. Fig. 1(b) presents the details of cladding air holes, where the hexagonal air hole spacing Λ is 4.18 μm, the rounding diameter of air holes (*Dc*) is 1.62 μm, rounded hexagons diameter (*d*) is 4.055 μm and the cladding air hole thickness *t* is 125 nm. The elliptical hollow core structure has the ellipse long axis length *A* of 13.2 μm and the ellipticity of 1.2, as shown in Fig. 1(c). There are totally 7 layers of the PBG cladding, and Fig. 1(d)–(f) show 3 different refractive indices distributions as Bragg layers within the PBG cladding. n_1, n_2, and n_3 represent the refractive indices of doped silica materials in the cladding.

In Fig. 1(a), the fiber actually becomes a conventional PBGF with uniform silica capillary within the cladding, named as PBGF1, while the pure silica walls are supposed to have uniform refractive index of $n_1 = 1.45$, as shown in the blue color in Fig. 1. In Fig. 1(d) to Fig. 1(f), another two varied refractive indices Bragg layers are introduced into the cladding. The lower refractive index of $n_2 = 1.44$ is illustrated in red color while the increased index of $n_3 = 1.46$ in green color. In Fig. 1(d), n_1, n_2, and n_3 are introduced into the inner three layers, the middle 4th layer and the outer three layers respectively, named as PBGF2. In Fig. 1(e), n_1, n_2, and n_3 are introduced into the inner two layers, the middle three layers and the outer two layers respectively, named as PBGF3. In Fig. 1(f), n_1, n_2, n_3 are introduced into the inner single layer, the middle 5 layers and the outer single layer respectively, named as PBGF4.

It is acknowledged that the weakly varied concave refractive index distribution in the silica capillary could be directly produced from the boron, germanium, fluorine or aluminum dopant [25],

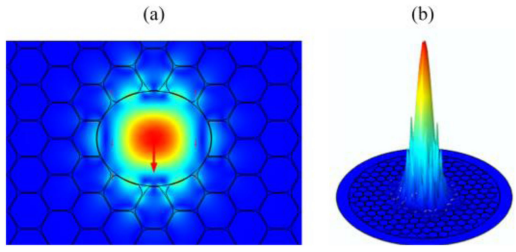

Fig. 2. Normalized optical field distributions at $\lambda = 1550$ nm for the fundamental mode of the designed fiber: (a) in vertical polarization; (b) 3D intensity profile.

[26]. By modifying doping elements and concentration in the silica glass, the refractive indices of the silica capillary could be selectively obtained and from 1.44 to1.46.

The cross section of the PBGF is divided into homogeneous subspaces that uses the finite-element method (FEM) with the perfectly matched layer (PML) boundary condition to solve Maxwell's equations. FEM could allow design flexibility and is currently an acknowledged numerical method to study HC-PBGFs. The PML boundary condition is employed, which has been proved to accurate and reliable in literatures [20]–[23]. From Maxwell's equations the following vectoral wave equation is derived as:

$$\nabla \times \left([s]^{-1} \nabla \times \vec{E} \right) - k_0^2 n^2 [s] \vec{E} = 0 \tag{1}$$

with

$$[s] = \begin{bmatrix} s_y/s_x & 0 & 0 \\ 0 & s_x/s_y & 0 \\ 0 & 0 & s_x s_y \end{bmatrix} \tag{2}$$

where $k_0 = 2\pi/\lambda$ is the wave number in the vacuum and λ is the wavelength, n is the refractive index, *[s]* is the perfectly matched layer boundary matrix, s_y and s_x are PML parameters, E is the electronic filed.

Fig. 2 shows the normalized field distribution at $\lambda = 1550$ nm for the fundamental mode in the BL-PBGF structure. The matrix system is solved by FEM and the effective refractive index neff of fundamental mode can be obtained. In general, the birefringence of the PCF is defined as [27]:

$$B = |n^x_{eff} - n^y_{eff}| \tag{3}$$

where $n^x{}_{eff}$ and $n^y{}_{eff}$ are the effective refractive indices of the X-polarized and Y-polarized fundamental modes. The confinement loss L is defined as [23]:

$$L = \frac{20}{\ln 10} \frac{2\pi}{\lambda} Im(n_{eff}) \quad (dB/m) \tag{4}$$

where n_{eff} is the effective refractive index and λ is the optical wavelength.

Bending loss is derived from the change of effective refractive index while bending. In the bent fiber the inner area of the fiber cross section is squeezed and the outside is stretched. Then the refractive index of the outside area increases and the uneven distribution of refractive index make the modes leak easily, i.e., bending loss. The change of refractive index is defined by [23]:

$$n'(x, y) = n_0(x, y) \left(1 + \frac{x \cos\theta + y \sin\theta}{R} \right) \tag{5}$$

where R is bending radius, n_0 and n' are the refractive index before bending and after bending, x and y represent the transversal and longitudinal distance from the fiber center, θ is the angle between bending axis and X axis. The bending loss is similarly defined by Eq. (4) while n_{eff} after bending can be obtained by Eq. (5). In this paper, the bending axis is X axis, i.e., θ is 0.

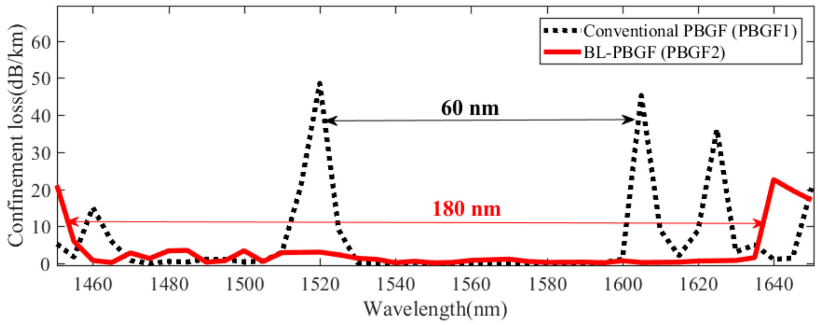

Fig. 3. Wavelength dependence of confinement loss of the conventional PBGF1 (in black) and PBGF2 (in red) between 1450 nm and1650 nm.

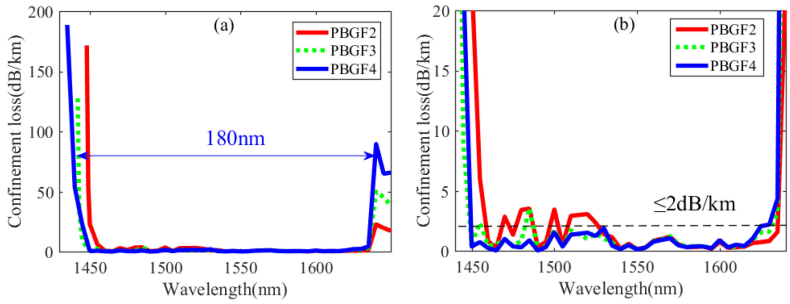

Fig. 4. (a) Wavelength dependence of confinement losses for PBGF2 (in red), PBGF3 (in green), and PBGF4 (in blue) between 1450 nm and1650 nm; (b) detailed loss data below 2 dB/km of these three BL-PBGFs with the wavelength range.

3. Optical Characteristics Analysis

The simulation analysis of the confinement loss, bending loss, birefringence and other characteristics is conducted to explore and illustrate unique features of these BL-PBGFs with concave-index cladding. The conventional PBGF without Bragg layer cladding is also considered for comparison in this section.

3.1 Confinement Loss

The confinement loss data of the BL-PBGF and the conventional PBGF (PBGF1) of y-polarized fundamental mode are obtained and shown in Fig. 3. As for the conventional PBGF1 (in black), it is obvious that the low loss bandwidth around 1550 nm is about 60 nm and the max loss value exceeds 50 dB/km, while the BL-PBGF (PBGF2) in red color has a considerably three times wider bandwidth of about 180 nm with low loss transmission. The confinement loss of PBGF2 is basically below 5 dB/km in the wavelength range of 1455 nm to 1635 nm. It is believed that, because different cladding refractive indices manifest respective photonic bandgaps and loss peaks, the combination of three refractive indices layers in the cladding could restrain and reduce these loss peaks, leading to the beneficial wideband low loss wavelength range. Hence the confinement loss of the BL-PBGF exhibits a significant beneficial bandwidth compared to the conventional PBGF.

Fig. 4 shows confinement loss data of three modified concave-index cladding BL-PBGFs with varied refractive indices layers. Fig. 4(a) shows the entire fiber transmission with low confinement loss band for PBGF2 (in red), PBGF3 (in green), and PBGF4 (in blue). Fig. 4(b) details the loss data between 1450 nm and 1650 nm for comparison between these fibers, which is more concerned for S to L bands implementation. It is obvious that all BL-PBGFs have considerably ultrawide low loss bands over 180 nm, while PBGF3 and PBGF4 exhibit even lower loss compared to PBGF2. As for PBGF4 (in blue), the loss data under 2 dB/km ranges from the overall ultrawide band and the loss

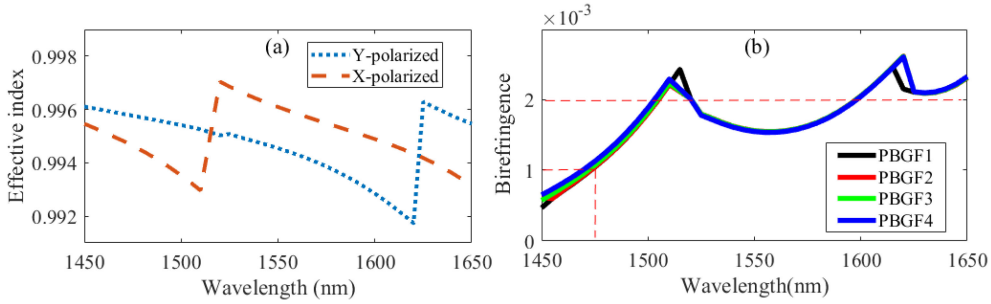

Fig. 5. (a) The effective refractive index of x-polarized and y-polarized modes vs. wavelength for BL-PBGF4 between 1450 nm and 1650 nm; (b) wavelength dependence of birefringence for the conventional PBGF1 (in black), PBGF2 (in red), PBGF3 (in green) and PBGF4 (in blue).

below 1 dB/km locates in the entire C band. Beside the low loss feature, the ultrawide bandwidth design is also beneficial for practical implementation, despite of possible photonic bandgap shifts from dimensional errors in fiber fabrication. The proposed BL-PBGFs with concave-index cladding could eliminate all loss peaks absolutely in the entire S to L bands and allow ultrawide low loss transmission bandwidths compared to the conventional PBGF.

3.2 Birefringence

The birefringence and effective refractive index data of the proposed BL-PBGFs and the conventional PBGF are all analyzed and discussed. Fig. 5(a) shows the effective refractive index of x-polarized and y-polarized modes for the BL-PBGF4 and all the conventional PBGF and the proposed BL-PBGFs have similar effective index. The discontinuities in the trace correspond to positions where one polarized mode undergoes an anti-crossing event [28]. Fig. 5(b) shows the general birefringence with the order of 10^{-3} from 1450 nm to 1650 nm for the conventional PBGF1 (in black), PBGF2 (in red), PBGF3 (in green) and PBGF4 (in blue). Principally the birefringence has an increasing trend at longer wavelength, and there exist abnormal conditions for individual wavelengths, not affecting general birefringence characteristics. The birefringence of the proposed concave-index BL-PBGFs is basically in line with the conventional PBGF and it exceeds 1.0×10^{-3} at the longer wavelength region beyond 1470 nm. The birefringence is about 2×10^{-3} between 1500 nm and 1650 nm, comparable to commercial PMFs.

3.3 Bending Loss and Birefringence Performance

The substantial application of PMF is widely acknowledged as the freestanding fiber coil in FOG [13]–[15]. Normally the optical fiber is winded into few centimeter radius sized coils. As for miniaturized fiber coils, the bending loss of the fiber is essential and need to be carefully investigated. Bend-induced loss at 1550 nm can be inferred by comparing the bending-induced effective index variation and is derived from Eq. (5).

Bending loss data of the proposed BL-BGFS are plotted in Fig. 6. Fig. 6(a) presents the bending loss with bending radius from 2 mm to 40 mm for the four BL-PBGFs. Generally, the current PMF could be normally coiled with several centimeter radius for FOG implementations. Here, Fig. 6(b) presents the detailed bending loss data from 12 mm to 40 mm, noted as the circled areas in Fig. 6(a). The bending loss of the proposed BL-PBGFs with concave-index cladding (PBGF2, PBGF3, PBGF4) are inclusively reduced from about 1 dB/km to below 0.2 dB/km. All BL-PBGFs exhibit slight oscillation behavior at around 20 mm bending radius, and it is analyzed mainly due to the coupling of surface modes and central fundamental modes.

More importantly, for applications in miniaturized freestanding fiber coil and small footprint FOG, the PMF could be necessarily coiled in tens of millimeters radius in size. The proposed hollow

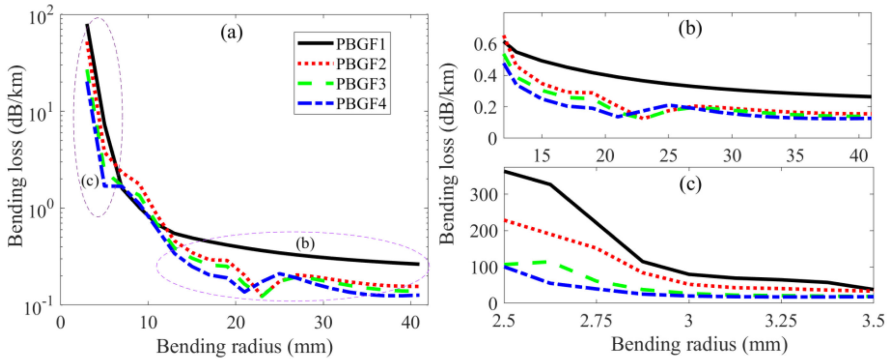

Fig. 6. (a) Bending loss dependence on the bending radius at 1550 nm for the conventional PBGF1 (in black), PBGF2 (in red), PBGF3 (in green), and PBGF4 (in blue); (b) detailed bending loss data with centimeters bending radius; (c) detailed bending loss data around 3 mm bending radius.

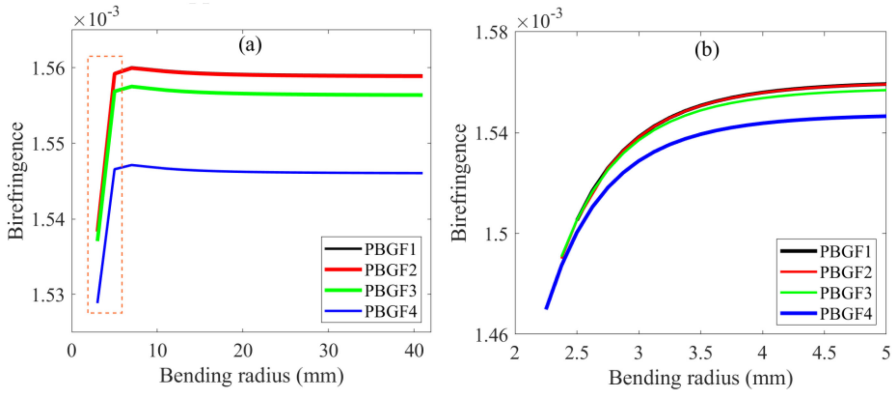

Fig. 7. (a) Birefringence as a function of the bending radius at 1550 nm; (b) the detailed bending loss data between 2 mm to 5 mm bending radius, for the conventional PBGF1 (in black), PBGF2 (in red), PBGF3 (in green), and PBGF4 (in blue).

core fiber with such small bending radius is investigated. Fig. 6(c) presents the detailed bending loss data around 3 mm, noted as the circled areas in Fig. 6(a). Between 2.5 mm and 3.5 mm, the bending loss of PBGF3 and PBGF4 are below one third of the conventional PBGF (PBGF1), and PBGF4 exhibits the most favorable low bending loss. With 2.75 mm bending radius, the bending loss of PBGF4 is about 40 dB/km, while the conventional PBGF (PBGF1) is over 220 dB/km. Hence, the proposed BL-PBGFs with concave-index cladding exhibit significant benefits in terms of the bending loss compared to the conventional PCF at both centimeters' radius and millimeters' radius.

The birefringence property of the BL-PBGFs at 1550 nm with varied bending radius are also shown in Fig. 7. As shown in Fig. 7(a), birefringence of the four PBGFs can completely stay around 1.56×10^{-3} although PBGF4 exhibits slightly lower value. Meanwhile, these BL-PBGFs can be coiled at bending radius beyond 4 mm without birefringence degradation. In case of miniature fiber coils, the bending radius could reach at millimeters level, and Fig. 7(b) details the birefringence data between 2 mm and 5 mm (the red dashed box in Fig. 7(a)). Birefringence of the BL-PBGFs begins to decrease with the bending radius below 4 mm, but still remains above 1.47×10^{-3} which can meet requirements for miniature FOG applications.

Considering the wavelength dependence of bending performance, Fig. 8 presents the confinement loss and birefringence varied with wavelengths for the straight PBGF4 and bent PBGF4 with 30 mm bending radius in the wavelength range of interest. The confinement loss of bent PBGF4

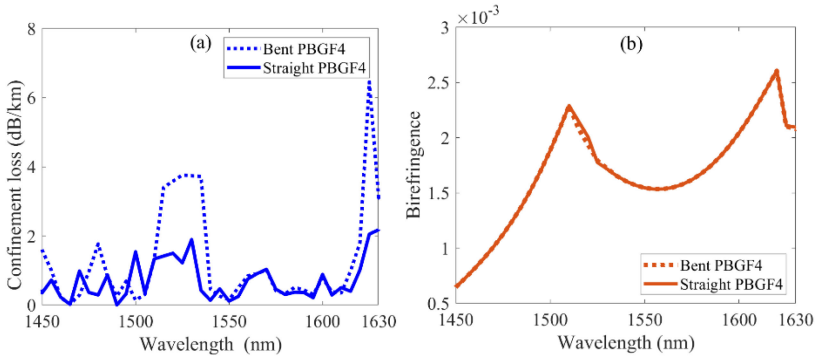

Fig. 8. Wavelength dependence of (a) bending loss and (b) birefringence at 30 mm bending radius for the straight PBGF4 (solid line) and bent PBFG4 (dash line).

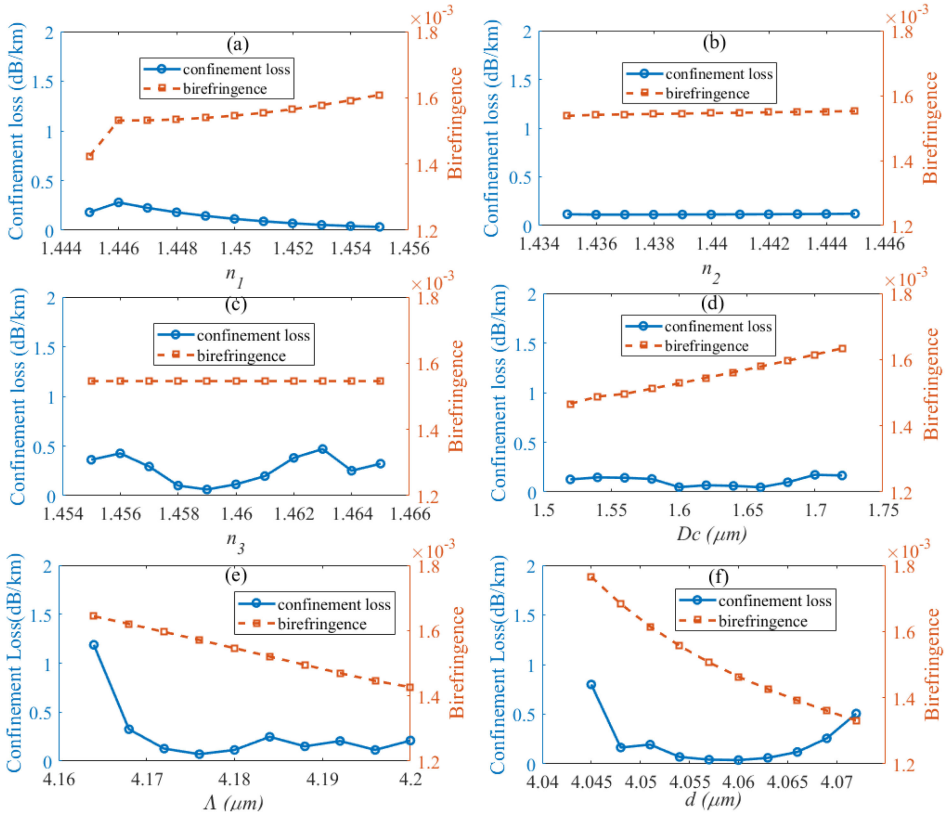

Fig. 9. Dependence of the confinement loss (blue curve and left axis) and birefringence (red curve and right axis) on fiber parameters at 1550 nm wavelength for PBGF4: (a) n_1; (b) n_2; (c) n_3; (d) Dc; (e) Λ; (f) d.

rises due to the bending geometry, but mostly stays below 4 dB/km in the ultrawide wavelength range. The birefringence of bent PBGF4 is also consistent with the straight fiber scenario, as shown in Fig. 8(b). It is concluded from the data that the proposed BL-PBGF manifests unique bending resistance feature due to the concave-index Bragg layer cladding and can maintain the anti-bending features within the ultra-wide wavelengths range, providing noteworthy potentials in miniature freestanding fiber coil and small footprint FOG applications.

TABLE 1
Optical Transmission Characteristics Comparison Between Several Previous Reported HC-PBGFs[a]

Researchers	Principle	Loss (dB/km)	Bandwidth (nm)	Birefringence	Bending Resistance	Type[b]
Chen in 2004 [6]	Anisotropy PBG	~ 1500	125	2.51×10^{-2}	×	Exp.
Fini in 2014 [7]	PBG + hollow 7-cell shunt	<10	14	2.2×10^{-4}	×	Exp.
Michieletto in 2014 [8]	PBG + cladding defects	~ 60	100	1×10^{-3}	×	Exp.
Serrão in 2013 [9]	PBG+ reduced air holes	<1	38	PDL>20 dB/m	×	Sim.
Chen in 2016 [10]	PBG + quasi-elliptical core	<20	130	4.6×10^{-4}	×	Sim.
Cai in 2020 [11]	Thin-diameter PBG	<15	150	1.2×10^{-4}	×	Sim.
This work	PBG+ Bragg layer	<2	180	1.55×10^{-3}	√	Sim.

[a]Derived from the data in the references and literatures.
[b]Type indicates whether the work is mainly about experiment or simulation.

4. Sensitivity and Tolerance Analysis

To ensure the practical feasibility of the proposed holey fiber topology, it is vital to examine in a detailed way the sensitivity of the structure on the design parameters. Such analysis will inform the prospective reader on the impact of structural tolerances on the performance of the fabricated structure. Specifically, we analyze the sensitivity of the loss and birefringence to the tolerances of structural parameters for PBGF4, since PBGF4 shows the ideal low confinement loss and anti-bending characteristics according to Section 3.

The influence of refractive indices (n_1, n_2, n_3), the rounding radius of cladding air holes (Dc), hexagonal air hole spacing (Λ) and rounded hexagons diameter (d) on confinement loss and birefringence at 1550 nm are analyzed and illustrated in Fig. 9. It is implied that the confinement loss keeps virtually constant with n_2 and fluctuates slightly with the other parameters. The outer cladding refractive index n_3 has utmost impact on confinement loss than other refractive indices (n_1, n_2). As for geometry parameters (Λ, d, Dc), Λ and d have greater effect on confinement loss than Dc. The birefringence behaves insensitive to refractive indices n_2 and n_3, since the cladding layers with n_2 and n_3 are located far from the central core and have limited effect on the geometrical birefringence. It is critical that, within the estimated tolerance, i.e., ±0.004 for refractive indices, ±0.2 microns for Dc, as well as ±15 nanometers for Λ and d, the proposed BL-PBGF could keep the wideband confinement loss below 1 dB/km and the birefringence above 1.4×10^{-3}, showing potential for practical holey fiber fabrication and implementations.

Furthermore, considering the varied refractive indices silica capillaries, the index contrast is below 0.7% and is feasible to fabricate by varied doping elements and concentration in silica capillaries through the chemical vapor deposition. Thermal expansion and mechanical tension of adjacent capillaries are basically identical because of the low 0.7% index contrast. Diffusion may occur at contacted membranes of two different capillaries while refractive indices within the same capillaries are basically kept uniform. In the simulation, refractive index distribution profiles have already been smoothed and utilized instead of the ideal stepped profiles with practical consideration. By using the typical stack and draw method [29], the proposed fiber may be fabricated in reality.

In general, Table 1 shows the HC-PBGF comparison of optical characteristics between this work and previously reported literatures.

5. Conclusion

In this paper, the wideband highly-birefringent anti-bending Bragg layered photonic bandgap fiber (BL-PBGF) with concave-index cladding is proposed and theoretically demonstrated, by incorpo-

rating photonic bandgap effect with Bragg effect, for the first time to the best of our knowledge. The confinement loss, birefringence, and bending loss characteristics are analyzed and compared with the conventional PBGF. The proposed BL-PBGF has low confinement loss under 2 dB/km for over 180 nm bandwidth, as well as limited bending loss which is below one third of the conventional PBGF. Meanwhile, its birefringence is in line with the commercial PMF and can meet the requirements of minimized optical fiber gyro. This unique concave refractive index BL-PBGF has broad advantages and great potential in fields of advanced optical fiber sensing applications.

References

[1] I. Kaminow, "Polarization in optical fibers," *IEEE J. Quantum Electron.*, vol. QE-17, no. 1, pp. 15–22, Jan. 1981.
[2] G. D. Pitt *et al.*, "Optical-fibre sensors," *IEE Proc. J. (Optoelectron).*, vol. 132, pp. 214–248, Aug. 1985.
[3] N. Anjum, P. C. Sreekanth, and J. Nayak, "Fiber optic sensors and optical sensing technology," in *Proc. Int. Conf. Elect., Electron., Optim. Techn.*, 2016, pp. 3884–3891.
[4] R. Saha, M. M. Hossain M. E. Rahaman, and H. S. Mondal, "Design and analysis of high birefringence and nonlinearity with small confinement loss photonic crystal fiber," *Front. Optoelectron.*, vol. 12, pp. 165–173, 2019.
[5] H. Valtna-Lukner, J. Repän, S. M. Valdma, and P. Piksarv, "Endlessly single-mode photonic crystal fiber as a high resolution probe," *Appl. Opt.*, vol. 55, pp. 9407–9411, Nov. 2016.
[6] X. Chen *et al.*, "Highly birefringent hollow-core photonic bandgap fiber," *Opt. Exp.*, vol. 12, no. 16, pp. 3888–3893, Aug. 2004.
[7] J. Fini *et al.*, "Polarization maintaining single-mode low-loss hollow-core fibres," *Nature Commun.*, vol. 5, Oct. 2014, Art. no. 5085.
[8] M. Michieletto, J. K. Lyngsø, J. Lægsgaard, and O. Bang, "Cladding defects in hollow core fibers for surface mode suppression and improved birefringence," *Opt. Exp.*, vol. 22, pp. 23324–23332, Sep. 2014.
[9] V. A. Serrão, and M. A. R. Franco, "A new approach to obtain single-polarization hollow-core photonic bandgap fiber," in *Proc. SPIE*, vol. 8794, 2013, Art. no. 879428. [Online] Available: https://doi.org/10.1117/12.2025849
[10] K. Chen, C. Wang, H. Hu, X. Shu, and C. Liu, "A single-mode polarization maintaining hollow core photonic bandgap fiber," *IEEE Photon. Technol. Lett.*, vol. 28, no. 22, pp. 2617–2620, Nov. 2016.
[11] H. Cai *et al.*, "Thin-diameter polarization maintaining hollow-core photonic bandgap fiber for fiber optic gyroscope," *Opt. Fiber Technol.*, vol. 55, Mar. 2020, Art. no. 102141.
[12] M. N. Hossen, M. Ferdous, K. Ahmed, M. A. Khalek, S. Chakma, and B. K. Paul, "Single polarization photonic crystal fiber filter based on surface plasmon resonance," *Front. Optoelectron.*, vol. 12, pp. 157–164, Jun. 2019.
[13] S. Blin, H. K. Kim, M. J. F. Digonnet, and G. S. Kino, "Reduced thermal sensitivity of a fiber-optic gyroscope using an air-core photonic-bandgap fiber," *J. Lightw. Technol.*, vol. 25, no. 3, pp. 861–865, Mar. 2007.
[14] T. A. Morris, and M. J. F. Digonnet, "Broadened-laser-driven polarization-maintaining hollow-core fiber optic gyroscope," *J. Lightw. Technol.*, vol. 38, no. 4, pp. 905–911, Feb. 2020.
[15] H. Jiao, L. Feng, J. Wang, K. Wang, and Z. Yang, "Transmissive single-beam-splitter resonator optic gyro based on a hollow-core photonic-crystal fiber," *Opt. Lett.*, vol. 42, no. 15, pp. 3016–3019, Aug. 2017.
[16] G. A. Sanders, B. Szafraniec, R. Y. Liu, C. L. Laskoskie, L. K. Strandjord, and G. Weed, "Fiber optic gyros for space, marine, and aviation applications," in *Proc. SPIE 2837*, 1996, pp. 61–71.
[17] J. Nayak, "Fiber-optic gyroscopes: From design to production," *Appl. Opt.*, vol. 50, no. 25, pp. E152–E161, Sep. 2011.
[18] J. Sakai, "Analytical expression of core and cladding material losses effect in Bragg fibers using the perturbation theory," *J. Opt. Soc. Amer. B.*, vol. 28, no. 11, pp. 2755–2764, Nov. 2011.
[19] S. G. Johnson *et al.*, "Low-loss asymptotically single-mode propagation in large-core omniguide fibers," *Opt. Exp.*, vol. 9, no. 13, pp. 748–779, Dec. 2001.
[20] A. Cucinotta, S. Selleri, L. Vincetti, and M. Zoboli, "Holey fiber analysis through the finite-element method," *IEEE Photon. Technol. Lett.*, vol. 14, no. 11, pp. 1530–1532, Nov. 2002.
[21] K. Saitoh, M. Koshiba, and S. Member, "Full-vectorial imaginary distance beam propagation method based on a finite element scheme: Application to photonic crystal fibers," *IEEE J. Quantum Electron.*, vol. 38, pp. 927–933, Aug. 2002.
[22] K. Saitoh, Y. Sato, and M. Koshiba, "Coupling characteristics of dual-core photonic crystal fiber couplers," *Opt. Exp.*, vol. 11, no. 24, pp. 3188–3195, Jan. 2004.
[23] Y. Qin, H. Yang, P. Jiang, F. Gui, W. Caiyang, and B. Cao, "Design and analysis for a bend-resistant and large-mode-area photonic crystal fiber with hybrid cladding," *Appl. Opt.*, vol. 57, no. 14, pp. 3976–3982, May 2018.
[24] N. A. Mortensen, and M. D. Nielsen, "Modeling of realistic cladding structures for air-core photonic bandgapfibers," *Opt. Lett.*, vol. 29, no. 14, pp. 349–351, Feb. 2004.
[25] J. W. Fleming, and D. L. Wood, "Refractive index dispersion and related properties in fluorine doped silica," *Appl. Opt*, vol. 22, no. 19, pp. 3102–3104, Oct. 1983.
[26] V. M. Mashinsky *et al.*, "Germania-glass-core silica-glass-cladding modified chemical-vapor deposition optical fibers: Optical losses, photorefractivity, and Raman amplification," *Opt. Lett.*, vol. 29, no. 22, pp. 2596–2598, Nov. 2004.
[27] A. Ortigosa-Blanch *et al.*, "Highly birefringent photonic crystal fibers," *Opt. Lett.*, vol. 25, no. 18, pp. 1325–1327, Sep. 2000.
[28] P. J. Roberts *et al.*, "Design of low-loss and highly birefringent hollow-core photonic crystal fiber," *Opt. Exp.*, vol. 14, no. 16, pp. 7329–7341, Aug. 2006.
[29] M. N. Petrovich, F. Poletti, A. van Brakel, and D. J. Richardson, "Robustly single mode hollow core photonic bandgap fiber," *Opt. Exp.*, vol. 16, no. 6, pp. 4337–4346, Mar. 2008.